Monitoring vegetation change and their potential drivers in Yangtze River Basin of China from 1982 to 2015

Lili Xu [iD] · Guangming Yu · Zhenfa Tu · Yucui
Zhang · Nandin-Erdene Tsendbazar

Abstract Monitoring vegetation change and their potential drivers are important to environmental management. Previous studies on vegetation change detection and driver discrimination were two independent fields. Specifically, change detection methods focus on nonlinear and linear change behaviors, i.e., abrupt change (AC) and gradual change (GC). But driver discrimination studies mainly used linear coupling models which rarely concerned the nonlinear behaviors of vegetation. The two diagnoses need be treated as sequential flow because they have inner causality mechanisms. Furthermore, ACs concealed in time series may induce over/under-estimate contributions from human. We chose the Yangtze River Basin of China (YRB) as a study area, first separated ACs from GCs using breaks for additive and seasonal trend method, then discriminated drivers of GCs using optimized Restrend method. Results showed that (1) 2.83% of YRB were ACs with hotspots in 1998 (30.2%), 2003 (10.4%), and 2002 (7.6%); 66.7% of YRB experienced GC with 94.8% of which were

positive; and (2) climate induced more area but less dramatic GCs than human activities. Further analysis showed that temperature was the main climate driver to GCs, while human-induced GCs were related to local eco-policies. The widely occurring ACs in 1998 were related to the flooding catastrophe, while the dramatic ACs in sub-basin 12 in 2003 may result from urbanization. This paper provides clear insights on the vegetation changes and their drivers at a relatively long perspective (i.e., 34 years). Sequential combination of specifying different vegetation behaviors with driver analysis could improve driver characterizations, which is key to environmental assessment and management in YRB.

Keywords Abrupt change · Gradual change · Restrend · Naturogenic and anthropogenic drivers

L. Xu · G. Yu · Z. Tu · Y. Zhang
Key Laboratory for Geographical Process Analysis & Simulation of Hubei Province, Central China Normal University, Wuhan 430079, China

L. Xu (✉) · G. Yu · Z. Tu · Y. Zhang
College of Urban and Environmental Sciences, Central China Normal University, Wuhan 430079, China
e-mail: xulls@mail.ccnu.edu.cn

N.-E. Tsendbazar
Laboratory of Geo-Information Science and Remote Sensing, Wageningen University & Research, Droevendaalsesteeg 3, 6708 PB Wageningen, The Netherlands

Introduction

Profiling vegetation cover change and their drivers in a relatively longer period is essential for understanding evolutions and exchange mechanisms of involved elements in local man-land systems (Gries et al. 2019). On decades scale, climate variables and human activities are two main drivers that could deeply influence the vegetation cover on the Earth (Hao et al. 2018; Huang et al. 2016; Liu et al. 2018). Climate variables such as precipitation, temperature, and sun radiation drive the plant physiological processes such as photosynthesis, respiratory, and transpiration, while human activities, such as urbanization, deforestation, grazing prohibition policy,

reclamation of land from lakes, market fluctuation etc., could directly or indirectly change the processes of vegetation dynamic by modifying ecosystem composition and distribution (Xu et al. 2016). Although these above two drivers alternately or simultaneously drive and co-decide the direction of vegetation dynamic, they seldom serve an equal amount of impacts to local vegetation during longer period. Discriminating the relatively dominant driver would be helpful to uncover the evolution and interacting processes between local ecosystems and external interferences.

The remote-sensing vegetation index such as Normalized Difference Vegetation Index (NDVI) is one of the most common indicators for pixel-based analysis of vegetation change and their drivers on regional, continental, and planet scale (Ivits et al. 2013; Zhao et al. 2015). Previous studies on vegetation change detection and driver analysis focused on two separate themes. First, various change detection methods were developed to target non-linear or linear behaviors of vegetation, i.e., abrupt change (AC) and gradual change (GC), based on the hypothesis that ACs and GCs behave differently in time series NDVI trajectories (Kim et al. 2013). Specifically, parametric and non-parametric linear analysis (Mu et al. 2013; Zhao et al. 2012) and nonlinear detection methods (Wu et al. 2017) were designed to detect GCs and ACs, respectively. Trajectory-based statistical methods were designed to detect both GCs and ACs concealed in time series remote-sensing datasets. These methods are breaks for additive and seasonal trend (Bfast) (Verbesselt et al. 2010a; Zeileis et al. 2002; Zeileis et al. 2005), detecting breakpoints and estimating segments in trend method (Jamali et al. 2015), continuous change detection and classification method (Zhu and Woodcock 2013), and Landsat-based detection of trends in disturbance and recovery (Cohen et al. 2010; Kennedy et al. 2007; Kennedy et al. 2010). Second, driver discrimination studies mainly dedicated to developing different models based on linear models to integrate climate variables and human-related variables based on the hypothesis that climate and human activities are two main dominant drivers responsible for the decades-scale change of vegetation cover. One popular philosophy in current research is directly treating anthropogenic drivers (i.e., land cover transition) and climate factors as spatial-temporal covariates to explain vegetation change (Hawinkel 2019; Wen et al. 2017). However, one of the biggest challenges of these studies is the difficulty in explicating uncertainty due to mismatch in the spatial-temporal scale of different drivers. While the classic philosophy in most research of this field is to use indirect way to weight the dominant drivers by firstly simulating the potential relationship between climate and vegetation and then attribute the differences between potential vegetation status and real vegetation status to anthropogenic factors (Evans and Geerken 2004; Gu et al. 2017; Prince 2010; Wessels et al. 2007, 2012). But a challenge of these studies is that they built the model involving vegetation and climate variables mainly based on linear coupling relationship without considering the nonlinear behaviors of vegetation cover. For instance, the residual trend method (Restrend) (Li et al. 2012; Wessels et al. 2012; He et al. 2015), which is widely used to discriminate human-/climate-induced vegetation change, builds a model based on analyzing the trend of residuals in a vegetation-climate linear regression.

However, before characterizing the drivers of vegetation changes, it is necessary to separate ACs from GCs in advance. Two key reasons are as follows: first, studies about vegetation change detection and driver discrimination could be treated as a sequential chain process instead of two separate fields because of the causal relationships between them. ACs and GCs in vegetation should be treated differently because they may be driven by different factors with different complicated mechanisms. Specifically, ACs usually could be associated with human-induced land cover transitions such as deforestation, urbanization, land reclamation, or extremely climate events such as flood and drought (Forkel et al. 2013). While GCs usually happen gradually and continuously, which indicate gradual improvement or deterioration of plant coverage or species composition associated with global warming, soil erosion, fertilizing, irrigation, or nurturing (Coppin et al. 2004; Forkel et al. 2013; Jong et al. 2011), these kinds of behaviors could be related to climate gradual change or indirect human activities such as environmental management, policy alteration, or market fluctuation. Second, it has been proven that linear coupling models which are the basics of Restrend method would over/under-estimate contributions from human activities in case of ACs. In some extreme cases, ACs may directly result in anomaly residuals in the vegetation-climate regression model and therefore may lead to even opposite conclusions. A previous study (Qu et al. 2018) used a nonlinear method to detect AC year on a regional scale and separate the whole time series into former and later

periods. Then, it conducted Restrend with treating the former period as a reference period. However, it is unreal that each pixel in the study area has ACs simultaneously. Furthermore, ACs in the former or later period could also result in uncertainties in the linear model of Restrend. It is more reasonable to exclude the ACs in Restrend model and pixel-based trajectory analysis methods which are developed recently that could be used to target ACs before Restrend.

This study combined change detection model with driver analysis model by treating these two processes as a sequence flow to discover annual vegetation dynamics and their potential drivers. We chose the Yangtze River Basin of China (YRB) as study area. Firstly separated ACs from GC by Bfast model and then discriminated naturogenic and anthropogenic drivers in GCs using optimized Restrend model based on Global Monitoring and Simulation Research Group (GIMMS) NDVI3g datasets and climate datasets derived from 138 meteorological stations from 1982 to 2015. Results were demonstrated in the whole basin scale, 3 stream scale, and 12 sub-basin scale to elaborate the spatio-temporal heterogeneity in YRB. This paper provides pronounced insights on eco-evolution and corresponding external drivers in YRB at a relatively long perspective, which is meaningful for decision-making on environmental management and restoration of this area.

Materials and methods

Study area

The YRB (24°30′N~35°45′N; 90°33′E~122°25′E) covers an area about 18.8% of China's total land area with mountains (65.6%), hills (24%), and plains (10.4%) from west to east (Fig. 1). The climate in majority of YRB is subtropical monsoon climate with annual mean temperature that ranges from 12.6 to 28.0 °C and average annual precipitation up to 476 mm. According to the land cover map in 2001, there are mixed forest (35.9%), grassland (20.9%), cropland (19.8%), shrub (16.6%), evergreen needle leaf forest (1.3%), deciduous broadleaf forest (0.6%), evergreen broadleaf forest (0.5%), deciduous needle-leaf forest (0.1%), and non-vegetation area (4.2%).

High-speed urbanization started with the ambition of developing the 'Yangtze River Economic Belt' released by the Chinese government in 1990s (Cui et al. 2013).

Besides the fact that extreme weather events (e.g., severe storms, heatwaves, prolonged drought) increase during the past 30 years (Dufresne et al. 2013; Gold 2012; Leng et al. 2015; Mora et al. 2017), economic developments in YRB resulted in several serious environmental problems (Gao et al. 2013; Li et al. 2017). Therefore, it is necessary to describe vegetation change and their potential drivers in YRB. To elaborate the spatio-temporal heterogeneity of our results, we conducted analysis in 3 scales, i.e., the whole basin, 3 streams, and 12 sub-basins. The boarders of YRB and the definition of different streams/sub-basins are according to the announcement released by the Changjiang Water Resources Commission dispatched by the Ministry of Water Resources of the People's Republic of China (Table 1).

Data and data preprocessing

The GIMMS NDVI3g with the longest time series accumulation (1982~2015) was downloaded from the NASA website (http://glcf.umd.edu/data/gimms/). The datasets involve 816 phase images from January 1982 to December 2015 with 8-km spatial resolution and semi-monthly temporal resolutions. It has been subjected to radiation correction, set correction, and image enhancement and other preprocessing (Du et al. 2016). We firstly used the maximum value composite method to produce monthly NDVIs, then accumulated NDVIs from April to October each year to obtain the annual growing seasonal NDVI datasets (ASNDVI). Each time series ASNDVI trajectory (TSNDVI) has 34 points corresponding to the 34 years from 1982 to 2015. The TSNDVI could well record vegetation dynamic in a local and global scale and widely used in research about vegetation dynamic analysis (Forkel et al. 2013; Prajjwal and Bardan 2012),

Precipitation and temperature were treated as two representative vegetation-related climate variables in this paper. Monthly precipitation dataset (P) and monthly mean temperature dataset (T) from 1982 to 2015 were downloaded from the website of the China Meteorological Data Service Center (http://data.cma.cn/). Each dataset contains records of 138 meteorological stations located within the YRB. The quality of the datasets was tested and missing data at the beginning or end of the trajectory were replaced by the average value of those months in all other years with data while remaining missing data were filled using the linear interpolation
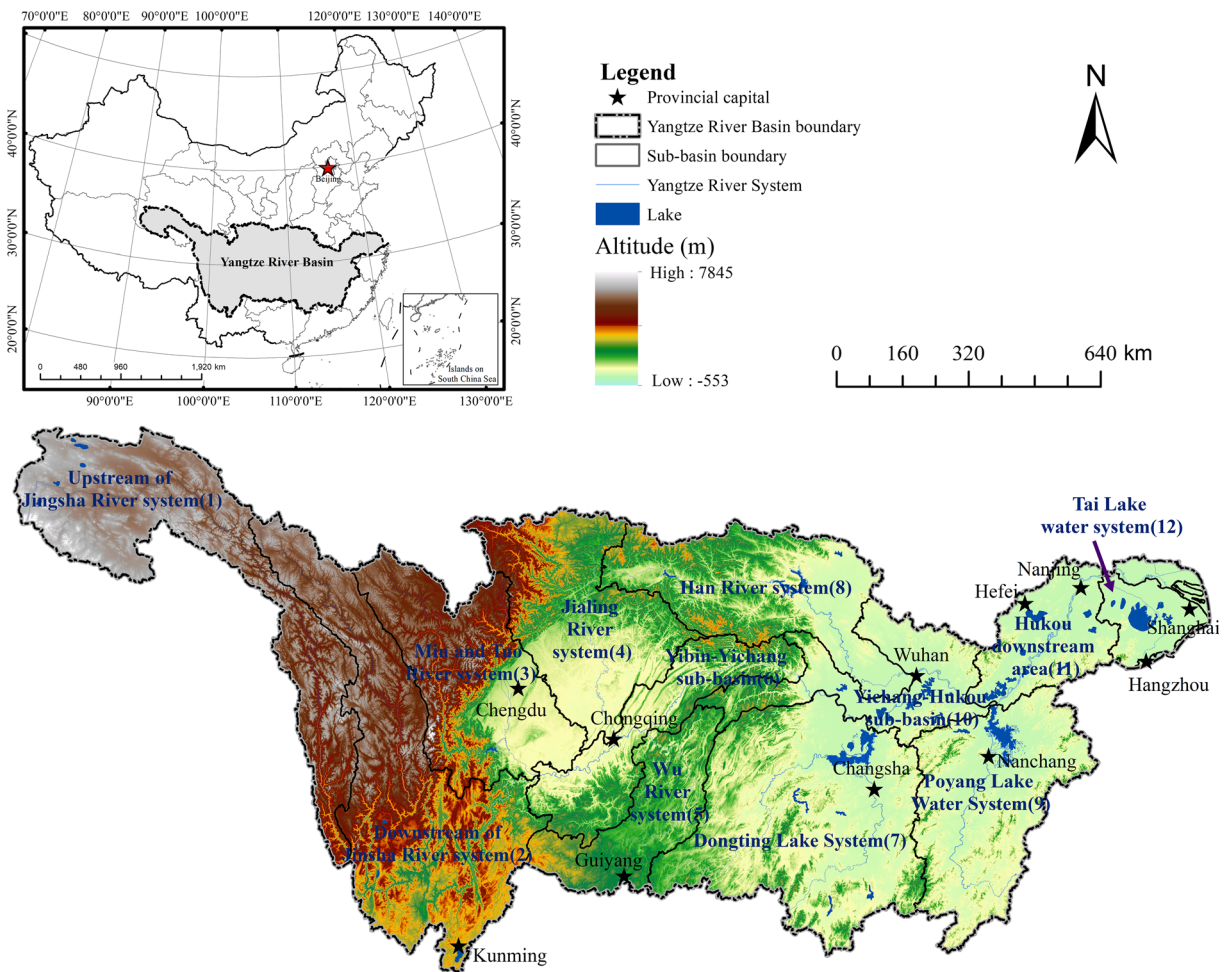
Fig. 1 Location of the YRB in China

Table 1 The sub-basins in YRB

Mark	Sub-basins	Streams
Sub-basin 1	The upstream of Jingsha River system	The upper stream (sub-basins 1~6)
Sub-basin 2	The downstream of Jingsha River system	
Sub-basin 3	The Min and Tuo River system	
Sub-basin 4	The Jialing River system	
Sub-basin 5	The Wu River system	
Sub-basin 6	The Yibing-Yichang water system	
Sub-basin 7	The Dongting lake system	The middle stream (sub-basins 7~10)
Sub-basin 8	The Han River system	
Sub-basin 9	The Poyang lake river system	
Sub-basin 10	Yichang-hukou sub-basin	
Sub-basin 11	The Hukou downstream area	The downstream (sub-basins 11~12)
Sub-basin 12	Taihu lake water system	

method (Hu et al. 2015). Because of the lag effect of vegetation growth to climate variable, 45 indices with different temporal combinations (Xu et al. 2018) were calculated for P and T, and then, the indices in each station were interpolated by the inverse distance weighting method to obtain overall 90 climate raster grids with the same resolution as the NDVI dataset. In each pixel, there are 45 T-series and 45 P-series from different temporal combinations.

The 1:1,000,000 scale ecological map for YRB, produced by the Chinese Academy of Sciences (2001), was used to identify ecological zones in the optimized Restrend method (Xu et al. 2018). The MCD12Q1 land cover maps of 2001 were obtained from the MODIS website (https://modis.gsfc.nasa.gov/about/), with processed yearly observation data from the Terra and Aqua satellites applied to depict land cover types. Annual cloud-free composite stable Defense Meteorological Satellite Program (DMSP)/Operational Linescan System (OLS) nighttime light brightness products from 1992 to 2012, which were widely used to investigate socioeconomic change and urbanization at different temporal-spatial scales, were downloaded from the website (https://ngdc.noaa.gov/eog/dmsp.html). The DMSP/OLS datasets under the WGS84 coordinate reference system were nocturnal luminosity with a 30×30 arc-second (approximately 0.8 km × 0.8 km at the 40°N area) spatial resolution ranging from 0 to 63. The original dataset was corrected by using empirical cross-correction based on binomial fitting to eliminate signal drift and degradation caused by different sensors and inter-annual fluctuation (Ma 2019). Point of interest (POI), i.e., pixels in the Tai lake system with a digital number (DN) larger than 50, were treated as human settlements according to previous related study (Shu et al. 2011). The human settlement time series from 2000 to 2009 was constructed by normalizing the number of POI pixels in corresponding years. Besides, the social-economy datasets of the Tai lake system, including the area of cropland and built-up land in Wuxi, Changzhou, and Suzhou, were obtained from local economic statistical datasets from 2000 to 2009.

Methods

Bfast method

The pixel-based Bfast method was used to detect GCs and ACs in TSNDVI from 1982 to 2015. The model

was developed from econometric models and had been proven to be a powerful method to detect structural changes in time series NDVI datasets on large scale (Verbesselt et al. 2010a, b). Bfast used iterative strategies to gradually find breakpoints based on a trend-seasonal decomposition model (Equation 1) and structural change detection model (Jong et al. 2013; Zeileis et al. 2002, 2005; Zeileis 2005).

$$y_t = a_1 + a_2 t + \sum_{j=1}^{k} r_j \sin\left(\frac{2\pi j t}{f} + \delta_j\right) + \varepsilon_t \qquad (1)$$

where y_t is the time-series observations, a_1 is the intercept, a_2 is the slope of the trend, r_j is the amplitude, δ_j is the phase (i.e., season), k is the harmonic terms, f is the frequency (e.g., $f = 12$ in the monthly precipitation series and monthly mean temperature series), and ε_t is the unobservable error at time t, i.e., standard deviation (σ).

The MOving SUMs (MOSUM) of the ordinary least square (OLS) residual process (OLS-MOSUM) was used to determine structural change breakpoints ($\alpha = 0.05$ in this study). The OLS-MOSUM process is sum of a fixed number of residuals in a temporal window whose size is determined by the bandwidth parameter (it was set to 0.15 in this study). The final output model was determined by a best-fit model, i.e., the Bayesian information criterion (BIC) in Equation 2.

$$BIC = 2\ln(L) + k \qquad (2)$$

Significant GCs were simultaneously derived by models based on trajectories without breakpoints. In detected pixels with GC, we also calculated change rate determined using Equations (3) and (4):

$$S_{\Delta NDVI} = \frac{(\beta \times t_n + a) - (\beta \times t_1 + a)}{\beta \times t_1 + a} \times 100 \qquad (3)$$

$$a = \overline{X} - \beta \times \bar{t} \qquad (4)$$

where $S_{\Delta NDVI}$ is the NDVI change rate (percentage of ASNDVI increase over the study period), $\overline{X}$ is the mean of the time series of NDVIs, $\bar{t}$ is the mean value of the dates, and t_1 and t_n are the start and end years of the time series, respectively.

Optimized Restrend method

In the GCs areas, we used 'optimized Restrend' (Xu et al. 2018) to discriminate naturogenic and

anthropogenic driving forces. This method inherited the philosophy of original Restrend and improved the original model by optimizing the strategy to automatically define flexible spatial homogeneous neighborhoods. Details of this method are described in the previous study of authors (Xu et al. 2018). First, pixel-based correlation analysis between TSNDVI and 90 climate series (i.e., 45 T-series and 45 P-series) were conducted to determine the most related period of T-series and P-series for ASNDVI.

Then, we used multiple regression analysis to build the pixel-level climate–vegetation model as in Equation 5:

$$y = \beta_0 + \beta_1 P + \beta_2 T, \tag{5}$$

where y is the TSNDVIs of the 'reference pixel', which refers to the maximum value ASNDVIs within the homogeneous spatial neighborhood of the target pixel; P and T are the normalized values of the most related P-series and T-series, respectively; and β_0, β_1, and β_2 are the parameters of the model. The location of a corresponding reference pixel for a specific pixel x was determined by three steps as described in the previous study (Xu et al. 2018).

Finally, the residual analysis was conducted. Residuals refer to the differential value between the potential ASNDVIs and the actual ASNDVIs. A significant decreasing or increasing trend in residuals indicated that vegetation change is driven mainly by human activities (Evans and Geerken 2004). If there was no trend in the residual series, changes that happened during the study period were driven mainly by climate change (Wessels et al. 2012).

Results

Separate ACs from GCs in YRB

ACs in YRB

There were 2.83% of the total area in YRB that went through significant ACs during the past 34 years. Figure 2 shows most of AC pixels commonly distributed along rivers such as Jingsha River and Xiang River, or around the top three freshwater lakes in YRB (i.e., Poyang, Dongting, and Tai Lake). The most intensive and dramatic ACs happened in plains of downstream,

which is the most developed and densely populated area in YRB.

As regards to the years of ACs, results showed that the ACs not equally happened in each year during the study period. The majority of ACs happened in the year 1998 (30.2%), then in 2003 (10.4%), and 2002 (7.6%). ACs that happened in these 3 years accounted for 48.2% of the total detected ACs (Fig. 3), which was a strong cue to indicate that ACs did not happen randomly and might be related to some specific events in these years.

The spatio-temporal distribution of ACs was quite various in different sub-basins. Figure 4 e shows detected ACs in different streams (upper stream > middle stream > downstream). It indicated that the upper stream of YRB experienced more dramatically external interferences than the downstream during the past 34 years. Although there were more ACs happened in the middle stream than in the downstream according to Fig. 4e, the downstream area deserved more attention because ACs in the downstream area located more concentrated than those in the middle stream. Further results in Fig. 4a showed that sub-basins 1, 12, and 7 had large areas with ACs with rates up to 21.0%, 18.4%, and 13.3% of total ACs, respectively, while sub-basins 8, 6, and 5 kept more stable ecosystems with ACs only up to 3.1%, 1.2%, and 0.1%, respectively.

Figures 4 b, c, and d further demonstrate that the main change years in the three typical sub-basins were obviously different. Specifically, Fig. 4b shows that the ACs in sub-basin 1 mainly happened in the year 1994. However, the main change years in the sub-basin 12 and the sub-basin 7 were 2003 and 1998, respectively (Fig. 4c and d). Compared with results in Fig. 3, ACs happened in 1998 on the YRB located in the middle stream and downstream, while ACs happened in 2002 and 2003 on the YRB that were mainly located in the downstream.

The change characteristics in the temporal field were also various in different sub-basins. The sub-basin 1 had ACs in almost every year. Excluding the most dramatic changes in 1994, there were still dramatic changes in 2008 and 2009 as shown in Fig. 4b. However, ACs in sub-basin 12 mostly happened in 2003 and partly concentrated in 1998 and 2002. We could, therefore, conclude an obvious periodical temporal pattern in this sub-basin according to Fig. 4c, that is, ACs are more common in the period 1982 to 2003 than the period 2003 to 2015. In sub-basin 7, almost all the ACs happened in the year 1998 and there were rare ACs in other years as shown in Fig. 4d.
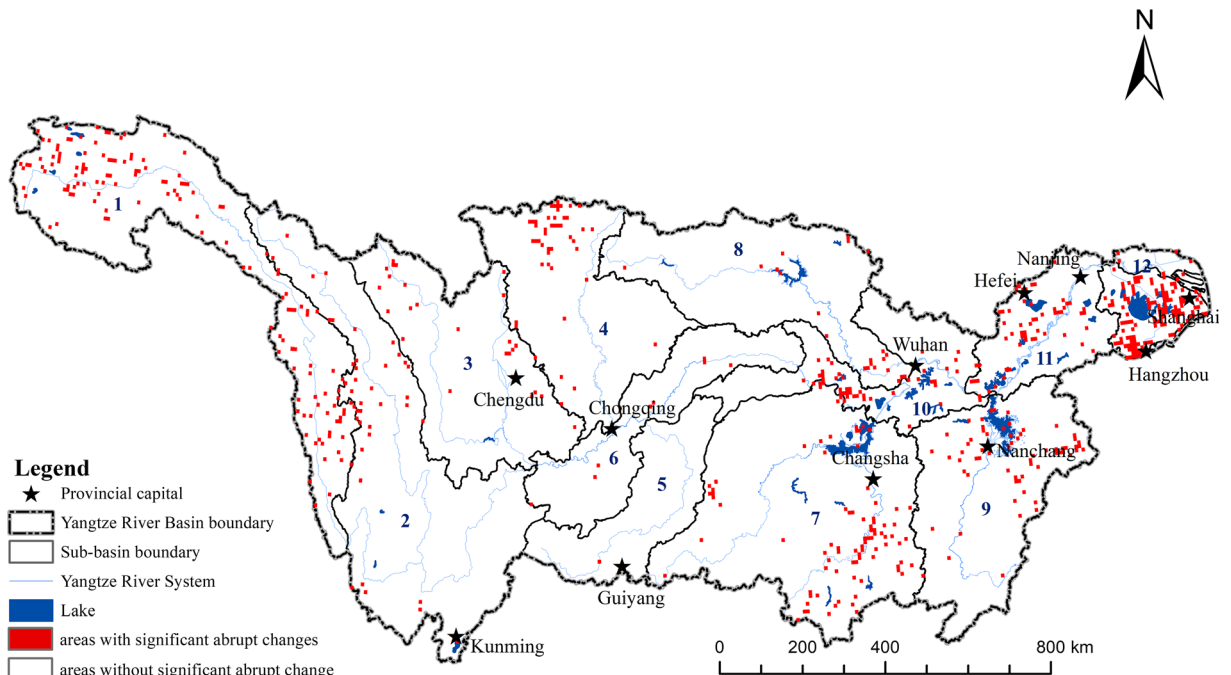
Fig. 2 ACs in YRB from 1982 to 2015

Figure 5 further shows the location of ACs in sub-basins 1, 12, and 7 in different years. It showed that ACs mainly happened around the city Shanghai in 2002 and 2003, while it happened mainly at the southwest of the sub-basin 12 in 1998 (Fig. 5b). However, the ACs mainly happened along the Xiang River in 1998 in sub-basin 7(Fig. 5d). In sub-basin 1, the ACs almost happened every year and there was dramatic AC that happened in 1994 (Fig. 5f).

GCs in YRB

From 1982 to 2015, the vegetation changes in YRB were mainly characterized by a significant increasing trend, which reflected the gradual improvement of vegetation coverage in the study area during the past 34 years ($y = 0.0177x - 27.385$, $R^2 = 0.49$). About 66.7% of YRB (1,190,692.2 km^2) showed significant GCs, within which there were 94.8% of the GCs that
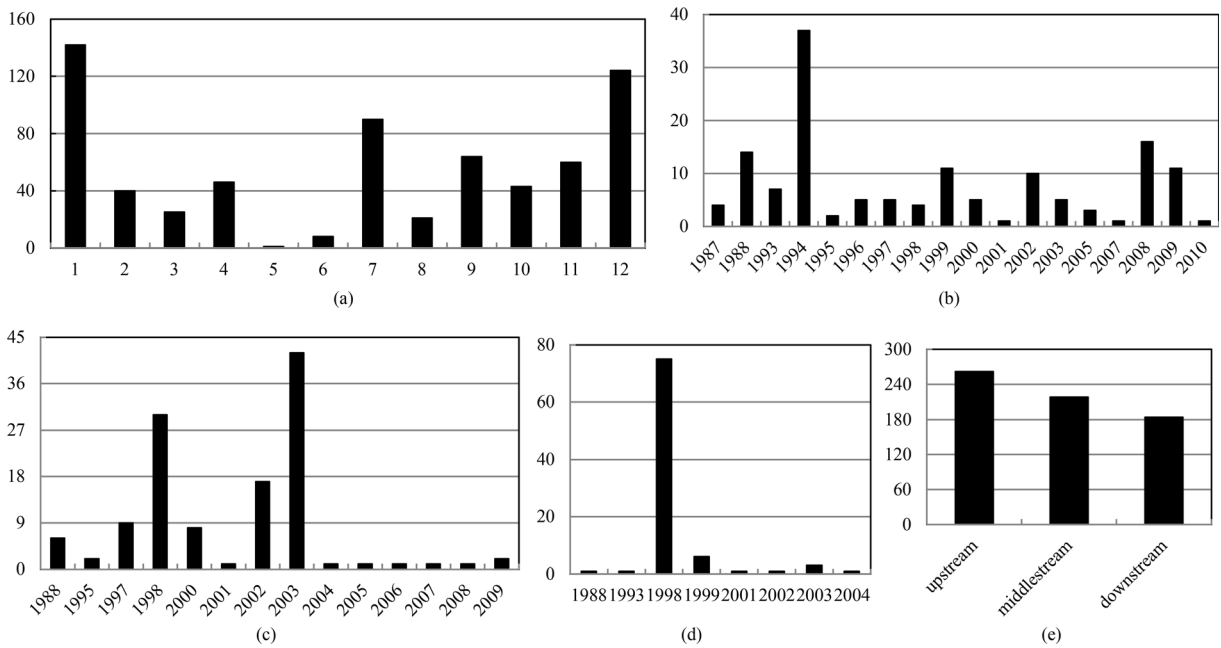
Fig. 3 Years of ACs in YRB from 1982 to 2015
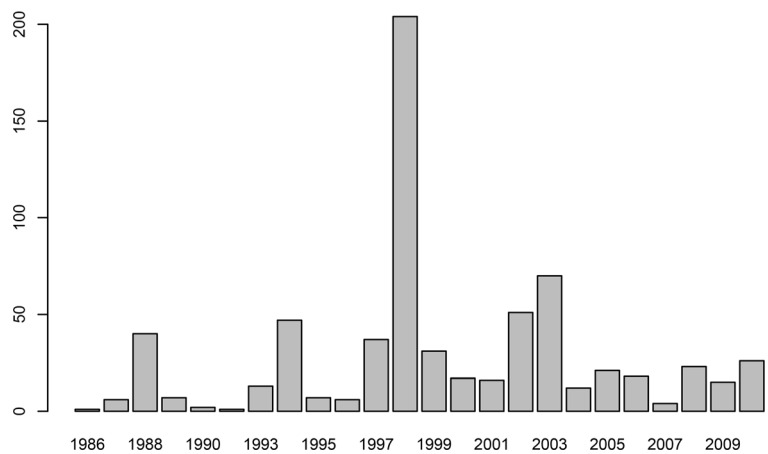
Fig. 4 Total number of pixels with ACs in YRB. **a** ACs in different sub-basins with marks as section 2.1; **b** AC years in sub-basin 1; **c** AC years in sub-basin 12; **d** AC years in sub-basin 7; **e** ACs in upper stream, middle stream, and downstream of YRB

showed positive trend and only 5.2% of the GC regions showed a negative trend (Fig. 6).

Change rates in different areas of YRB were not synchronous (Fig. 6). In the upper and middle streams, vegetation cover had a significant increase. But in the downstream, vegetation cover remained stable during past 34 years. The change rate in the middle stream ($y = 0.0244x - 40.038$, $R^2 = 0.50$) was higher than that of the whole YRB, while the change rate in the upper stream ($y = 0.018x - 28.147$, $R^2 = 0.49$) was closer to that of the whole YRB.

Strong spatial heterogeneity of GCs was demonstrated by sub-basin analysis. Results showed that vegetation cover in sub-basin 6 of the upper stream experienced the fastest increase ($y = 0.0313x - 53.561$, $R^2 = 0.55$), while vegetation cover in sub-basin 1 ($y = 0.004x - 3.4438$, $R^2 = 0.17$) and sub-basin 2 ($y = 0.008x - 8.3556$, $R^2 = 0.15$) experienced the slowest growth. Other areas such as sub-basin 5 ($y = 0.0273x - 45.549$, $R^2 = 0.44$), sub-basin 4 ($y = 0.0268x - 44.717$, $R^2 = 0.52$), and sub-basin 9 ($y = 0.0262x - 43.595$, $R^2 = 0.58$) in the middle stream also had a high change rate. It was especially noticeable that the average value of NDVIs in sub-basin 12 ($y = -0.0033x + 12.843$, $R^2 = 0.02$) showed a

negative trend, which contrasts to trends in all the rest sub-basins.

Although the change rate in the upper stream had the most consistency with that in the whole YRB during the past 34 years, it had the strongest spatial heterogeneity. Sub-basins with the highest change rates, such as sub-basins 6, 5, and 4, and the sub-basins with the lowest change rates (i.e., sub-basin 1) were all located in this area. The change characteristics in the middle stream had the weakest spatial heterogeneity and almost all the sub-basins increased simultaneously during the past 34 years. However, overall stable change in downstream ($y = 0.0034x + 0.2091$, $R^2 = 0.02$) was resulted by offset effect from the positive trend in sub-basin 11 and the negative trend in sub-basin 12.

As regard to the rates of GCs, the absolute value of increase rates in positive GC areas was overall higher than the absolute value of decrease rates in negative GC areas. A dramatic vegetation increase and a moderate vegetation decrease happened during the past 34 years. Specifically, in the positive GC areas, area with rate between 10 and 20% was the largest class with reaching 47.8% of the total positive GCs areas; area with rate between 0 and 10% was about 40%; area with rate between 20 and 40% accounted for 6.7%, and area with
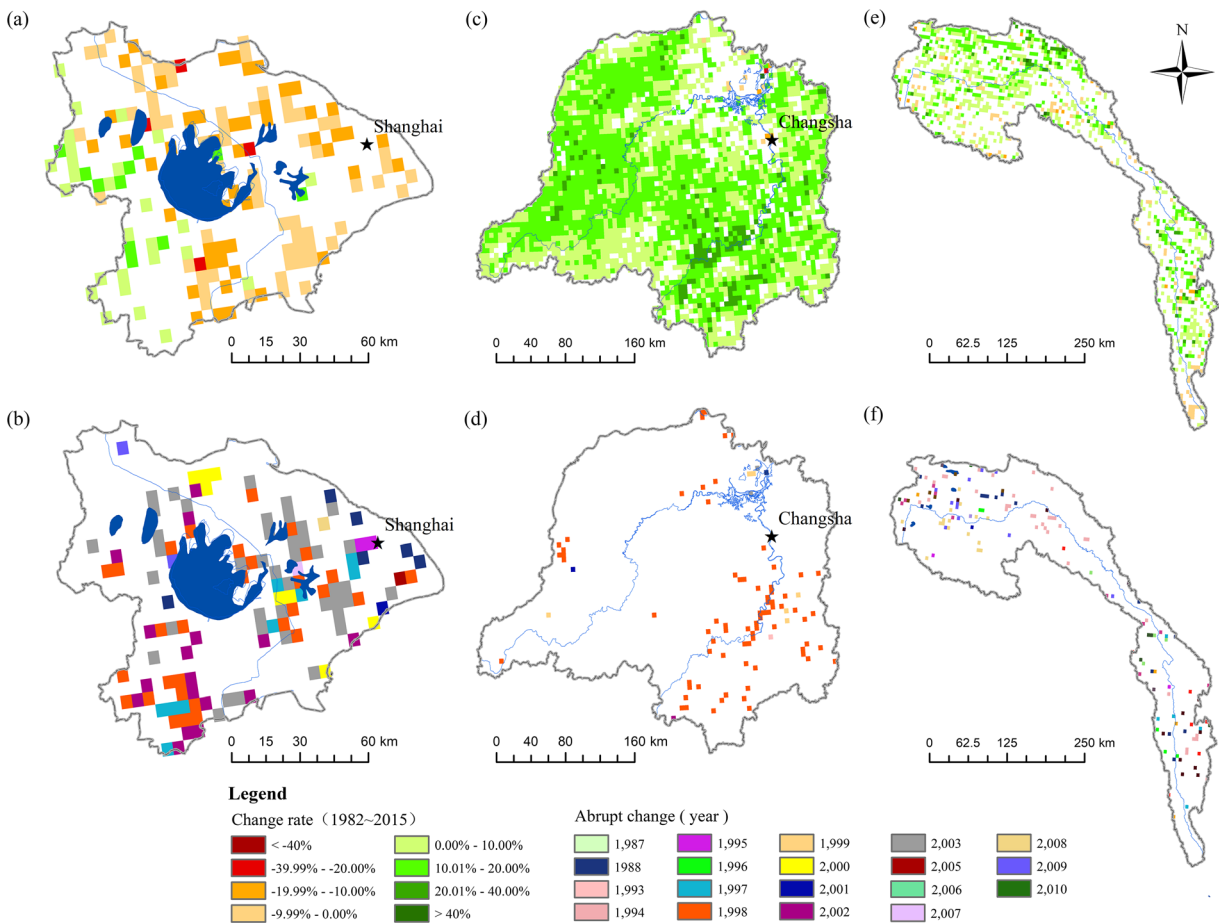
Fig. 5 ACs and TCs in different sub-basins of YRB. **a** TCs in sub-basin 12; **b** AC areas and years in sub-basin 12; **c** TCs in sub-basin 7; **d** AC areas and years in sub-basin 7; **e** TCs in sub-basin 1; **f** AC areas and years in sub-basin 1

rate above 40% was only 0.23%. While in the negative GC areas, area with rate between −10% and 0 was the largest class with reaching 3.7% of the total negative GC areas; area with rate between −20 and −10% accounted for about 1.3%; area with rate below −40% was only 0.01%; there were only 0.17% of negative GC areas with rate between −40 and −20% (Table 2).

Positive GCs were mainly concentrated in the middle stream and the eastern upper stream (Fig. 6). Vegetation cover in the middle stream was mainly positive and there were large areas with GC rate exceeding 10%. The most significant vegetation increases happened in sub-basin 2 and in sub-basin 6. The change rate in these areas usually exceeded 20%. It was worth noting that the most significant vegetation decreases happened in sub-basins 1, 3, and 12.

Table 2 further evidences that about 50% of the total GC changes in sub-basins such as sub-basins 1, 3, and

the 10 were between 0 and 10%. It indicated that although large areas in these sub-basins went through significant GCs, the degree of vegetation change was not dramatic. It was also noticeable that pixel-based vegetation cover changes in sub-basins 4, 5, and 6 all showed increasing and there were no vegetation degradations that happened in these areas during the past 34 years. In addition, there were 55.7%, 62.0%, and 58.7% of GC rates concentrated between 10 and 20% with a relatively intense degree of vegetation change. There was even 12.1% of the change in the sub-basin 4 increased over 20%, which was the most typical area with rapid vegetation cover growth in the YRB.

The vegetation change in sub-basin 12 was the most complicated in the study area: on the one hand, about 60.85% of GC areas showed vegetation decrease and there were 30.2% of GC area decrease more than −20%; on the other hand, this area had the highest percentage of
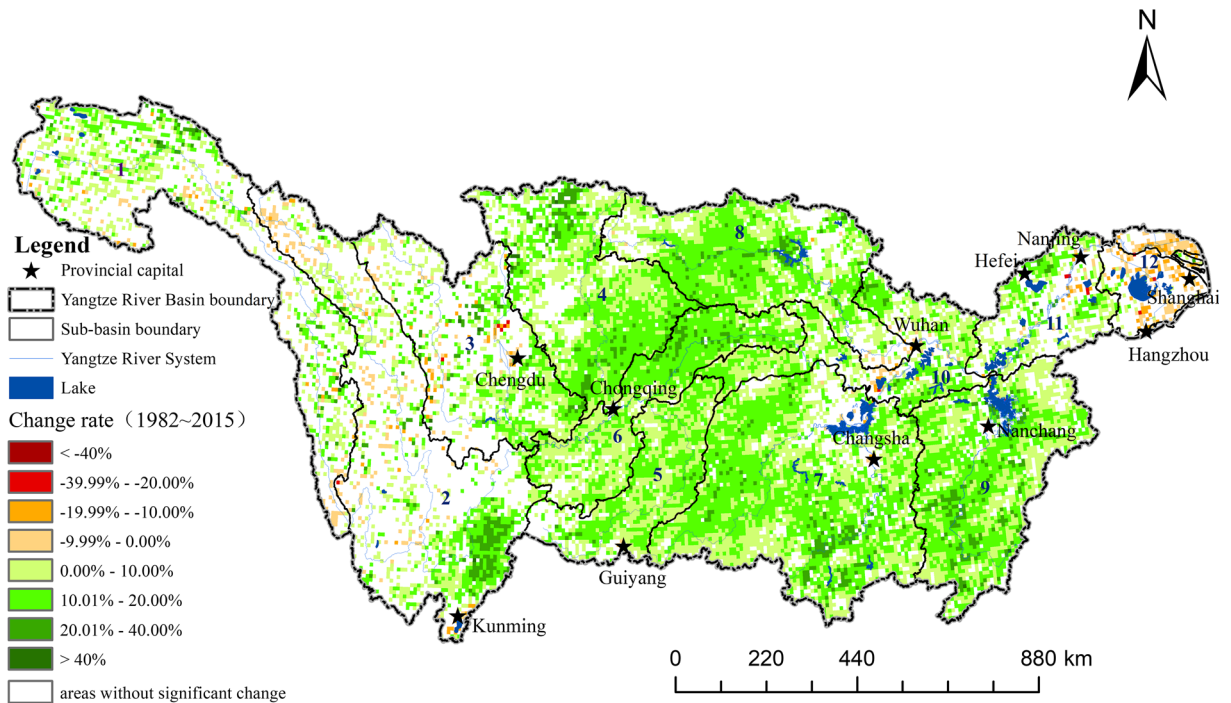
Fig. 6 GCs in YRB from 1982 to 2015

decrease area with GC rate over 40%. It went through coexisted and complex increase and decrease of GC (Table 1). Areas with a negative rate between − 10% and 0 accounted for 39.7% of the total GCs in the basin, while the proportion of areas with a rate between 0 and

10% of the total change area was 17.1%. The sum of areas with these two types of moderate change rates had exceeded more than half of the total change area. In areas with drastic changes, there were 30.1% of total change areas with a rate below − 10%, while at the same

Table 2 Change rates in GC study area

Sub-basins	Increase (%)				Decrease (%)			
	> 40%	20~40%	10~20%	0~10%	− 10~0%	− 20~− 10%	− 40~− 20%	< − 40%
1	0.59	5.84	31.13	48.98	11.17	2.20	0.08	0.00
2	0.08	11.25	32.66	39.33	14.43	2.02	0.23	0.00
3	0.40	4.55	38.91	47.82	4.55	3.07	0.69	0.00
4	0.40	11.70	51.66	36.19	0.06	0.00	0.00	0.00
5	0.00	1.94	61.98	35.69	0.39	0.00	0.00	0.00
6	0.00	8.88	58.68	32.44	0.00	0.00	0.00	0.00
7	0.03	4.94	55.09	39.36	0.34	0.20	0.03	0.00
8	0.00	6.06	54.45	38.00	1.19	0.30	0.00	0.00
9	0.64	9.08	47.96	41.95	0.16	0.05	0.11	0.05
10	0.00	2.62	46.53	47.13	2.62	1.01	0.10	0.00
11	0.16	4.04	32.97	44.48	11.82	5.29	1.24	0.00
12	1.01	1.01	11.06	17.09	39.70	28.64	1.51	0.00
Overall	0.23	6.72	47.84	40.03	3.72	1.27	0.17	0.01

Note: the marks of sub-basin records corresponding to the mark of 12 sub-basins in Table 1

time, there were 13.1% of total change areas with rate more than 10%.

Dominant drivers in GCs areas

Results of optimized Restrend showed that climate factors (54.1%) contributed more to GCs than human activities (45.9%). The vegetation changes driven by these two different factors may have different characteristics of spatial agglomeration. In general, human-induced GCs had stronger spatial agglomeration than climate-induced GCs. The latter located evenly and scattered throughout the whole basin (Fig. 7 a and b).

Human-induced GCs mainly happened in the middle stream (Figs. 7a and 9a), and most of them turned to have a positive trend, especially in sub-basins 8 and 5. Human-induced negative GCs were mainly in sub-basin 12 of downstream (Fig. 7c). However, climate-induced GCs located evenly in each sub-basin (Fig. 9a), with climate-induced negative GCs mainly located in the upper stream of YRB (Fig. 7b).

Human activities influence vegetation dynamics in a more dramatic way than climate factors because absolute change rates in human-induced GCs are obviously higher than absolute change rates in climate-induced GCs. As shown in Fig. 7 c and d, majority of human-induced greening areas increased by more than 20%, while the majority of climate-induced greening areas increased by 10~20%. At the same time, majority of human-induced browning area decreased $-10\sim-19\%$ and more, while the majority of climate-induced browning area decreased $-9\%\sim0$.

Discussion

Specific climate and human-induced drivers in GCs

Correlation analysis between different climate variables and vegetation cover in Fig. 8 further demonstrated that GCs were more controlled by temperature than by precipitation in the study area. This finding is corresponding to results in previous studies. Cui et al. (2019) found that the overall increase of vegetation cover in YRB was closely correlated with temperature extremes (i.e., maximum temperature and minimum temperature). Yuan et al. (2019a). further proved that the start of growing season (SOS) of vegetation in YRB was the key period which is more sensitive to

temperature than to precipitation. The precipitation-related vegetation decrease mainly happened in the north part of sub-basin 8, north part of sub-basin 6, and areas between Xiang River and Gan River($\alpha <$ 0.05). Meanwhile, the precipitation-related vegetation increases mainly located in the north area of sub-basin 1. It is indicated that excessive precipitation may have a negative effect on vegetation cover in areas with enough water resources such as the middle stream and downstream, while it may have positive effect on vegetation cover in arid/ semi-arid area such as northern sub-basin 1. Figures 8 a and c also show that the decrease in vegetation cover in the sub-basins 4 and 12 had a significant negative correlation with temperature. The Hengduan Mountain area was typical because of the significant negative influence of both precipitation and temperature. In the majority of northern sub-basin 1, both precipitation and temperature had a significant positive influence to vegetation growth during the past 34 years.

As overlaying two layers, i.e., human-induced GCs (Fig. 7a) and the land cover map of 2001, it indicated that human-induced GCs mainly happened in forestland (50.7%), and then in farmland (27.1%) and grassland (21.0%). Changes that happened in these three classes overall accounted for 98.8% of total human-induced GCs. In YRB, grassland land cover is mainly in the upper streams, while farmland and forestland mainly located in the middle stream. The downstream is the most developed area with plenty of urban/built-up areas. Excluding the dramatic ACs happened in downstream which could be more directly related to human-induced land cover transitions, it seems that the GCs in middle stream could be also more induced by human activities than climate in an indirect way. Figure 9 a clearly demonstrates that the human-induced areas are mainly located in sub-basins 5, 7, 8, and 9 in the middle stream. Previous research (Hu et al. 2019) proved that grain production in the middle stream of YRB increased dramatically from 1990 to 2015 because of the increasing sown area, agriculture fertilizer, and population.

Besides, the eco-policies about regulating three types of national key ecological function areas (NKEFAs) in YRB since 2010 also contributed to GCs (Fig. 9d). The main reason for setting these NKEFAs is to protect and restore the local environment. In different NKEFAs, different policies and strategies were implemented with different extents of human intervention, according to their specific ecological situation and environmental
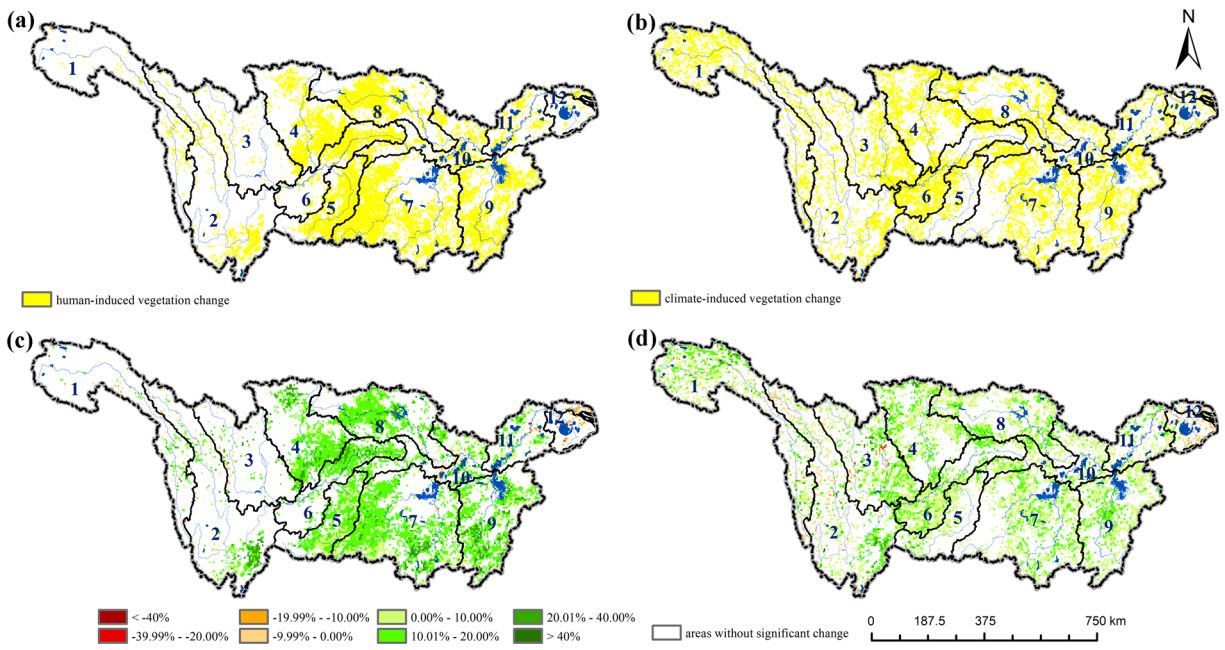
Fig. 7 **a** Human-induced vegetation change; **b** climate-induced vegetation change; **c** change rates in human-induced area; **d** change rate in climate-induced area

problems. Results in Fig. 9c showed areas of human/climate driving GCs in different NKEFAs, which could be correspondingly confirmed by different extents of human intervention form eco-policies. Specifically, in the soil and water conservation area, more GCs area related to human activities (Fig. 9c). Figures 6 and 7 a

and b show that northern sub-area 6 has the most relative higher and more dramatic influence from human activities than climate. Correspondingly, eco-policies in this NKEFA were more focused on 'restoration': (1) promoting water-saving irrigation and rainwater gathering system, developing dry farming and water-saving
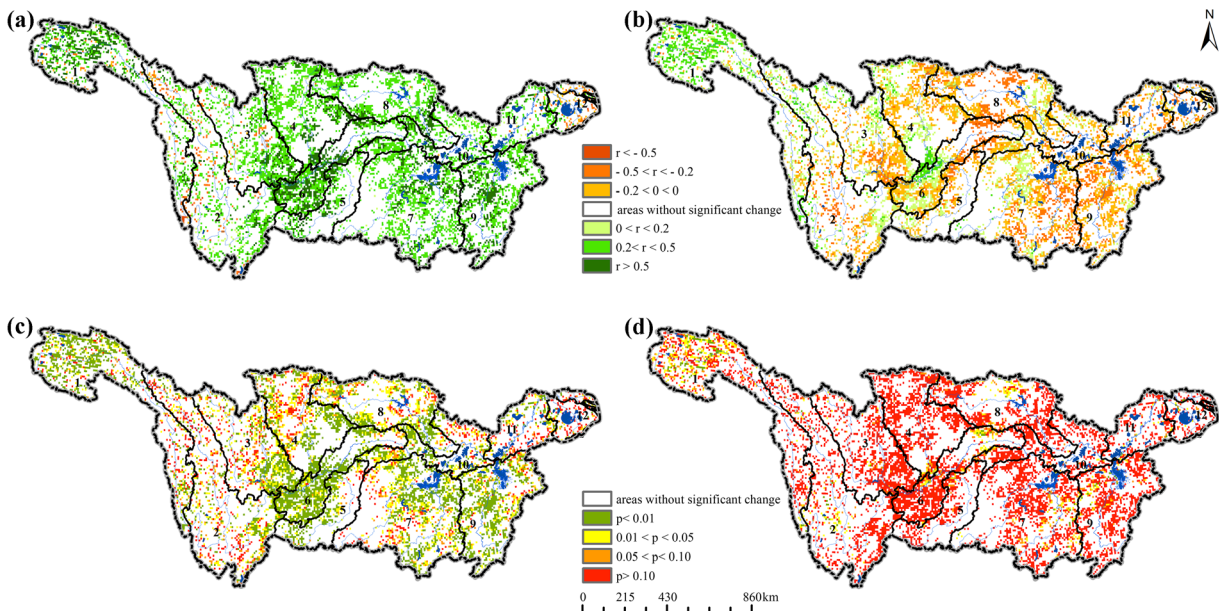

Fig. 8 **a** The correlation coefficient (*r*) between temperature and NDVI; **b** the correlation coefficient (*r*) between precipitation and NDVI; **c** statistical significance (*p*) of *r* between temperature and NDVI; **d** statistical significance (*p*) of *r* between precipitation and NDVI
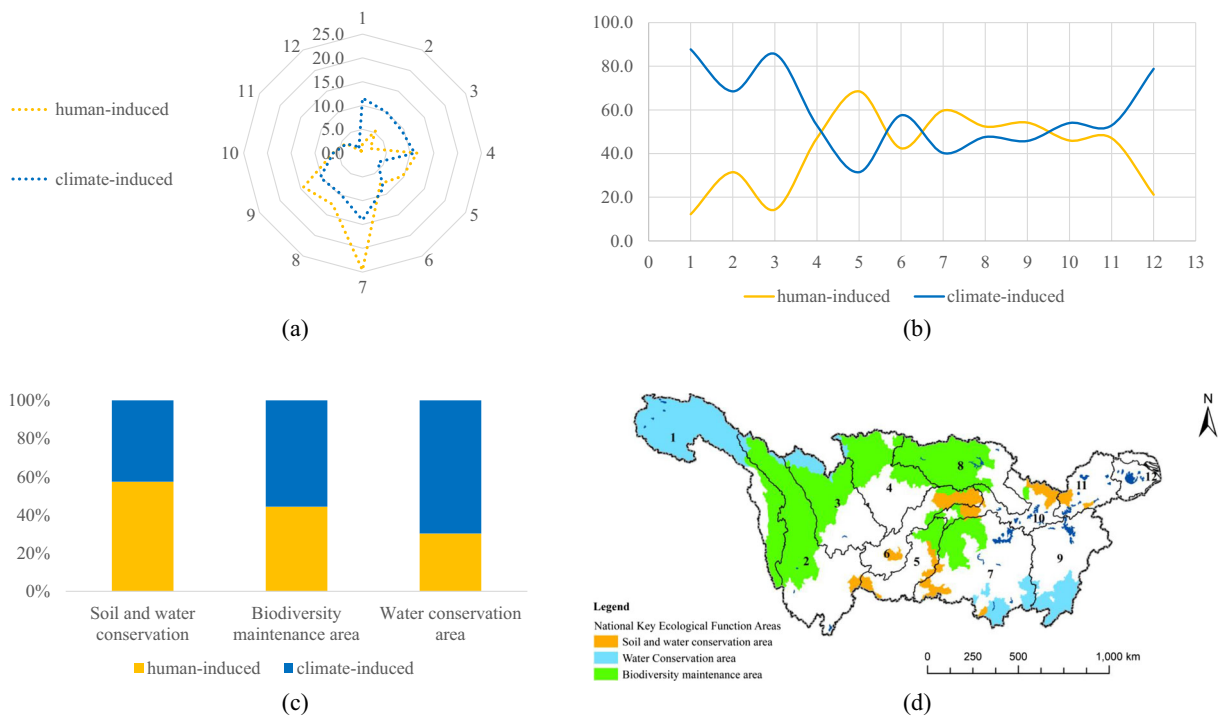
(a)

(b)

(c)

(d)

Fig. 9 **a** Percentages of human/climate-induced area in 12 sub-basins; **b** the relative percentage of human/climate driving area in 12 sub-basins; **c** the relative percentage of human/climate driving area in three types of NKEFAs; **d** NKEFAs in YRB

agriculture, limiting steep slope reclamation, and over-load grazing; (2) strengthening the comprehensive management of small watersheds, i.e., implement mountain closure, grazing prohibition, and restore degraded vegetation; (3) strengthening the supervision of energy and mineral resources development and construction projects, increase the efforts of mine environment remediation and restoration, and minimize the new soil erosion caused by human factors; (4) broaden farmers 'income-increasing channels, solve farmers' long-term livelihoods. These deeply human-involved strategies, combined with climate factors, contributed to the GCs in this NKEFA (Fig. 9c). However, in the other two NKEFAs, the main policies were more focused on 'protection' with decreasing influence by human with less intervention. Therefore, the percentages of human-induced GCs areas were relatively low as shown in Fig. 9c.

The different performances of human/climate-induced GCs in the upper and middle stream (Fig. 9b) are also corresponding to the population distribution pattern. The sub-basins 1~3 in upper stream has the lowest residential density in YRB; therefore, most GCs were driven by climate. While in the middle stream, human activities contributed slightly more than climate

factors to GCs. The situation in downstream has another different scene; less GCs related to human may come from the fact that human activities here had more direct ways which related to the densely ACs, which are further discussed in section 4.2.

The importance of detecting ACs before Restrend

Although there were a relatively lower percentage (2.83%) of the area in YRB that went through significant ACs during the study period, it is still necessary to detect ACs before the driver discrimination processes because of two reasons. The first reason is that excluding of detected ACs from the driver discrimination processes could avoid possibilities of over/under-estimate human effects in the 2.83% of areas. ACs hidden in TSNDVI may influence the linear regression relationship between climate and vegetation, which is the basic of Restrend (Wang et al. 2018). Results, therefore, might be unreliable when these interferences happened. The second reason is that AC areas and AC years are also very important change signals for local eco-restoration and eco-management because these kinds of information can usually be related to specific human

activities or big natural disasters happened in the study area. Previous work (Qu et al. 2018) detects AC year (i.e., year 1994) on the regional scale, while in our results, we found that ACs in 1994 mainly happened in the sub-basin 1 (Fig. 4b) and AC years in the other sub-basins were obviously diverse. It seems that detection of ACs only on regional scale will not only induce uncertainty of results but also cover up the specific drivers in different sub-basins.

In YRB, the year 1998 is the most extraordinary year according to our analysis. About 30.2% of detected ACs happened in 1998 (Fig. 3). In the middle stream and the downstream, the year 1998 also should not be ignored (Fig. 4c, d). The widely happened ACs in 1998 may be caused by the extremely global flood disaster in YRB, which is the second-largest flood disaster in this century since the year 1954, according to the government's historical records. In 1998, the annual precipitation amount is about 1216.7 mm/m^2, with 11.5% higher than the multiyear average amount. While the land surface water amount is about $13,004 \times 10^8$ m^3, with 27.4% higher than the multiyear average amount. Furthermore, the large amounts of precipitation are abnormally concentrated in summer 1998. It is shown that about 358.6 million acres cultivated lands in YRB were underwater, within which about 295 million acres happened in the middle stream and the downstream during the flood.

According to Figs. 2 and 3, there are about 10.4% of detected ACs that happened in 2003 in YRB and most of them happened in sub-basin 12. Evidence in Figs. 4c and 5b further proved this claim. Change of vegetation cover usually could represent the change of land cover to some extent. The densely happened ACs in 2003 in sub-basin 12 may be related to land cover changes caused by high-speed urbanization in this area, which is also stressed by the previous study (Yuan et al. 2019b). According to statistical data in Wuxi, Changzhou, and Suzhou in this area from 2000 to 2009, the total area of cultivated land in this three areas decreased 25.2% from 7.0×10^5 to 5.2×10^5 ha; meanwhile, the total built-up area increased dramatically according to analysis of DMSP/OLS datasets (Fig. 10). The year 2003 is a key year with high speed of increasing of built-up area and decreasing of cultivated area.

Limitations and further research

This paper provides a knowledge background on eco-evolution and influences from external drivers at a relatively long perspective. It is therefore meaningful for decision making on management and restoration of the ecosystems in YRB. However, this paper has some weaknesses which could be the aim of future studies.

First, we treated vegetation change detection and discriminating drivers as a chain process based on the causalities between them. Trajectory analysis methods, i.e., Bfast, were conducted to detect ACs and GCs before Restrend to avoid over/under-estimation of contributions from human activities. However, Bfast is not sensitive to ACs happened in the beginning or end of the study period, which may cause uncertainties to some extent. In addition, detected ACs can hardly be defined the "from–to" land cover change; therefore, they could only be indirectly related to specific ecosystem changes or land cover conversion caused by human activities or extremely climate events (Xu et al. 2016). As a result, their potential drivers could only be indirectly verified instead of directly interpreted, which makes the procedure of driver discrimination in ACs less automatic. These weaknesses may be improved by developing change detection methods.

Second, we only involved precipitation and temperature as two representative vegetation-related climate variables in the optimized Restrend model. It may cause uncertainties where other climate variables such as solar radiation or wind related to the interface processes in the vegetation-climate system. This limitation could be developed by importing the philosophy of some complicated models based on earth-climate system. Validation is not only hard for the ACs, but it is also hard when it comes to validate the human-induced GC. In fact, GCs could be influenced by policies, local eco-organization, social activities, e.g., surrounding vegetation could be
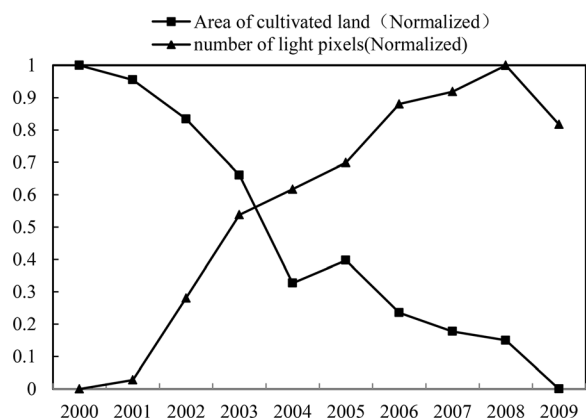

Fig. 10 Normalized area of cultivated land and urban land in Wuxi, Changzhou, and Suzhou of sub-basin 12 from 2000 to 2009

nurtured greening by a dam built in YRB, grassland biomass decrease caused by increasing livestock resulted from the increasing price of meat, patches of low yield farmland become scaled and organized foster land because of land-leveling policies in YRB, settlement shift and gathering caused by ecological migration policy, integrated basin management, and unified streams scheduling. All those indirect human activities possibly happen but hard to quantify and be combined with the pixel-based analysis. Social survey method could be used in the future to improve description of these factors.

Third, uncertainty of results could also be caused by our data sources. For example, the coarse spatial resolution of the NDVI dataset (i.e., 8 km) and relatively sparsely distributed meteorological stations make the results hard to be validated by other reference data. Seasonal accumulated remote sensing NDVI may ignore the fluctuation within seasonality of vegetation cover. Well-produced time-series Landsat archive with more fine spatial resolution or addition with a dataset from more dense meteorological stations may improve our study. Further research could be conducted on the Google earth engine platform, on which the easily accessible time series Landsat datasets, open-source change detection algorithms, and the powerful computer sever support could improve the certainty of our study. Satellite-based DMSP/OLS dataset was used to analyze temporal change of human settlements as an informative proxy way, based on the theory that there are notable quantitative relationships between anthropogenic nocturnal radiance and the degree of human activities at different scales (Ma 2018). However, the threshold method (i.e., DN > 50) we used to define human settlements in this paper may cause some uncertainty because of subjective perspective. Accurate human settlement dataset, site investigation, and questionnaire survey are all very important studies in future studies.

Conclusions

Studies on vegetation change detection and driver discrimination should be treated as follow-up flow for there are inner causality mechanisms between them. This paper chose YRB as the study area, aimed to profile vegetation dynamic and their potential dominant drivers from 1982 to 2015. Results were as follows:

There were 2.83% of the total area in YRB that went through significant AC, and the dramatic ACs happened in 3 years: 1998 (30.2%), 2003(10.4%), 2002 (7.6%); ACs were quite various in different sub-basins (upper stream > middle stream > downstream). Sub-basins 1, 12, and 7 had large ACs with rates up to 21.0%, 18.4%, and 13.3% of total ACs, respectively. ACs in sub-basin 1 mainly happened in the year 1994, and the main change years in sub-basins 12 and 7 were 2003 and 1998, respectively.

About 66.7% of YRB went through significant GCs during the past 34 years, within which there were 94.8% of GCs showed a positive trend (middle stream > upper stream > downstream) and only 5.2% of the GC regions showed a negative trend. In the upper and middle streams, vegetation cover increased significantly. But in the lower stream, vegetation cover remained stable. Sub-basin 6 in the upper stream went through the fastest growing of vegetation cover, while sub-basins 1 and 2 went through the slowest vegetation cover growing. The overall stable change in downstream was resulted by the offset effect from a positive trend in sub-basin 11 and a negative trend in sub-basin 12. Sub-basin 12 is the most serious area about vegetation decrease, compared with the rest sub-basins. But it is also the largest area with a rapid increase of vegetation (rate > 40%). It is indicated that in this area, human activities have the highest degree of impact and the impacts are mainly negative.

Climate factors (54.1%) contributed more to vegetation GCs than human activities (45.9%). The human-induced negative GCs were mainly in sub-basin 12. However, climate-induced GCs located evenly in each sub-basin and the climate-induced negative GCs mainly located in the upper stream. GC areas controlled by human activities may have more dramatic change rates comparing with the areas controlled by climate factors. GCs mainly happened in the forestland (50.7%), farmland (27.1%), and grassland (21.0%), which indicate the good effects of eco-projects in YRB. Majority of climate-induced GCs controlled by temperature, while human-induced GCs more related to different local eco-policies and residential density. Widely happened ACs in 1998 may be caused by the extremely global flood disaster in YRB and the densely happened ACs in 2003 in sub-basin 12 may be related to land cover change caused by high-speed urbanization in this area. The above results indicate strong spatial and temporal heterogeneous.

Although there were a relatively lower percentage (2.83%) of the area in YRB that went through significant ACs, it is necessary to separate ACs from GCs

before Restrend model. Weaknesses may be improved by developing change detection methods and using the philosophy of some complicated models based on earth-climate system. Accumulating accurate human settlement datasets, site investigation, and questionnaire survey are important in future studies. Future models could be conducted on the Google earth engine platform to improve the certainties of our results.

References

Cohen, W. B., Yang, Z., & Kennedy, R. (2010). Detecting trends in forest disturbance and recovery using yearly Landsat time series: 2. TimeSync-Tools for calibration and validation. *Remote Sensing of Environment, 114*, 2911–2924. https://doi.org/10.1016/j.rse.2010.07.010.

Coppin, P., Jonckheere, K. Nackaerts, Muys B., & Lambin E. (2004). Digital change detection methods in ecosystem monitoring: a review. *International Journal of Remote Sensing, 25*(9), 1565–1596. https://doi.org/10.1080/0143116031000101675 .

Cui, L., Gao, C., Zhao, X., Ma, Q., Zhang, M., Li, W., Song, H., Wang, Y., Li, S., & Zhang, Y. (2013). Dynamics of the lakes in the middle and lower reaches of the Yangtze River basin, China, since late nineteenth century. *Environmental Monitoring and Assessment, 185*, 4005–4018. https://doi.org/10.1007/s10661-012-2845-0.

Cui, L., Wang, L., Qu, S., Singh, R. P., Lai, Z., & Yao, R. (2019). Spatiotemporal extremes of temperature and precipitation during 1960–2015 in the Yangtze River Basin (China) and impacts on vegetation dynamics. *Theoretical and Applied Climatology., 136*, 675–692. https://doi.org/10.1007/s00704-018-2519-0.

Du, J. Q., Shu, J., Zhao, C., Jia E., Wang L. X., Xiang B. Fang G. L., Liu W. L., & He P. (2016). Comparison of GIMMS NDVI3g and GIMMS NDVIg for monitoring vegetation activity and its responses to climate changes in Xinjiang during 1982-2006. *Acta Ecologica Sinica, 36*(21), 6738–6749. https://doi.org/10.5846/stxb201504190805 .

Dufresne, J. L., Foujols, M. A., Denvil, S., Caubel, A., Marti, O., Aumont, O., Balkanski, Y., Bekki, S., Bellenger, H., Benshila, R., Bony, S., Bopp, L., Braconnot, P., Brockmann, P., Cadule, P., Cheruy, F., Codron, F., Cozic, A., Cugnet, D., de Noblet, N., Duvel, J. P., Ethé, C., Fairhead, L., Fichefet, T., Flavoni, S., Friedlingstein, P.,

Grandpeix, J. Y., Guez, L., Guilyardi, E., Hauglustaine, D., Hourdin, F., Idelkadi, A., Ghattas, J., Joussaume, S., Kageyama, M., Krinner, G., Labetoulle, S., Lahellec, A., Lefebvre, M. P., Lefevre, F., Levy, C., Li, Z. X., Lloyd, J., Lott, F., Madec, G., Mancip, M., Marchand, M., Masson, S., Meurdesoif, Y., Mignot, J., Musat, I., Parouty, S., Polcher, J., Rio, C., Schulz, M., Swingedouw, D., Szopa, S., Talandier, C., Terray, P., Viovy, N., & Vuichard, N. (2013). Climate change projections using the IPSL-CM5 Earth System Model: from CMIP3 to CMIP5. *Climate Dynamics, 40*, 2123–2165. https://doi.org/10.1007/s00382-012-1636-1.

Evans, J., & Geerken, R. (2004). Discrimination between climate and human-induced dryland degradation. *Journal of Arid Environments, 57*(4), 535–554. https://doi.org/10.1016/S0140-1963(03)00121-6.

Forkel, M., Carvalhais, N., & Verbesselt, J. (2013). Trend change detection in NDVI time series: effects of inter-annual variability and methodology. *Remote Sensing, 5*(5), 2113–2144. https://doi.org/10.3390/rs5052113.

Gao, J., Zhang, Y., Guo, J., Jin F., & Zhang K. (2013). Occurrence of organotins in the Yangtze River and the Jialing River in the urban section of Chongqing, China. *Environmental Monitoring and Assessment, 185*, 3831–3837. https://doi.org/10.1007/s10661-012-2832-5 .

Gold, A. U. (2012). Global weirdness: Severe storms, deadly heat waves, relentless drought, rising seas, and the weather of the future. In *Reports of the National Center for Science Education.*

Gries, T., Redlin, M., & Ugarte, J. E. (2019). Human-induced climate change: the impact of land-use change. *Theoretical and Applied Climatology., 135*(3–4), 1031–1044. https://doi.org/10.1007/s00704-018-2422-8.

Gu, X., Xiao, Y., Yin, S., Pan, X., Niu, Y., Shao, J., Cui, Y., Zhang, Q., & Hao, Q. (2017). Natural and anthropogenic factors affecting the shallow groundwater quality in a typical irrigation area with reclaimed water, North China Plain. *Environmental Monitoring and Assessment, 189*, 514. https://doi.org/10.1007/s10661-017-6229-3.

Hao, L., Pan, C., Fang, D., Zhang, X., Zhou, D., Liu, P., Liu, Y., & Sun, G. (2018). Quantifying the effects of overgrazing on mountainous watershed vegetation dynamics under a changing climate. *Science of the Total Environment, 639*, 1408–1420. https://doi.org/10.1016/j.scitotenv.2018.05.224.

Hawinkel, P. (2019). *Modeling vegetation dynamics driven by climate variability and land use changes in Rwanda.* Web..

He, C., Tian, J., Gao, B., & Zhao, Y. (2015). Differentiating climate- and human-induced drivers of grassland degradation in the Liao River Basin, China. *Environmental Monitoring and Assessment, 187*, 4199. https://doi.org/10.1007/s10661-014-4199-2.

Hu Q., Pan F.F., Pan X.B., Zhang D., Li Q.Y., Pan Z.H., & Wei Y.R. (2015). Spatial analysis of climate change in Inner Mongolia during 1961–2012, China. *Applied Geography, 60*, 254–260. https://doi.org/10.1016/j.apgeog.2014.10.009.

Hu, H., Wang, J., Wang, Y., & Long X. (2019). Spatial-temporal pattern and influencing factors of grain production and food security at county level in the Yangtze River Basin from 1990 to 2015. *Resources and Environment in the Yangtze Basin (in Chinese), 28*(2), 359–367.

Huang, K., Zhang, Y., Zhu, J., Liu, Y., Zu, J., & Zhang, J. (2016). The influences of climate change and human activities on

vegetation dynamics in the Qinghai-Tibet Plateau. *Remote Sensing, 8*(10), 876. https://doi.org/10.3390/rs8100876.

Ivits, E., Cherlet, M., Sommer, S., & Mehl, W. (2013). Addressing the complexity in non-linear evolution of vegetation phenological change with time-series of remote sensing images. *Ecological Indicators, 26*, 49–60. https://doi.org/10.1016/j.ecolind.2012.10.012.

Jamali, S., Jönsson, P., Eklundh, L., Ardö, J., & Seaquist, J. (2015). Detecting changes in vegetation trends using time series segmentation. *Remote Sensing of Environment, 156*, 182–195. https://doi.org/10.1016/j.rse.2014.09.010.

Jong, R. D., Bruin, S. D., Wit, A. J. W. de, Schaepman, M.E., & Dent, D.L. (2011). Analysis of monotonic greening and browning trends from global NDVI time-series. *Remote Sensing of Environment, 115*, 692–702. https://doi.org/10.1016/j.rse.2010.10.011 .

Jong R. D., Verbesselt J., Zeileis A., et al. (2013). Shifts in global vegetation activity trends. *Remote Sensing, 5*(3), 1117–1133. https://doi.org/10.3390/rs5031117.

Kennedy, R. E., Cohen, W. B., & Schroeder, T. A. (2007). Trajectory-based change detection for automated characterization of forest disturbance dynamics. *Remote Sensing of Environment, 110*, 370–386. https://doi.org/10.1016/j.rse.2007.03.010.

Kennedy, R. E., Yang, Z., & Cohen, W. B. (2010). Detecting trends in forest disturbance and recovery using yearly Landsat time series: 1. LandTrendr-Temporal segmentation algorithms. *Remote Sensing of Environment, 114*, 2897–2910. https://doi.org/10.1016/j.rse.2010.07.008.

Kim, D. Y., Thomas, V., Olson, J., Williams, M., & Clements, N. (2013). Statistical trend and change-point analysis of land-cover-change patterns in East Africa. *International Journal of Remote Sensing, 34*(19), 6636–6650. https://doi.org/10.1080/01431161.2013.804224.

Leng, G., Tang, Q., & Rayburg, S. (2015). Climate change impacts on meteorological, agricultural and hydrological droughts in China. *Global and Planetary Change, 126*, 23–34. https://doi.org/10.1016/j.gloplacha.2015.01.003.

Li, A., Wu, J., & Huang, J. (2012). Distinguishing between human-induced and climate-driven vegetation changes: a critical application of RESTREND in Inner Mongolia. *Landscape Ecology, 27*(7), 969–982. https://doi.org/10.1007/s10980-012-9751-2.

Li, R., Feng, C., Wang, D., He, M., Hu, L., & Shen, Z. (2017). Effect of water flux and sediment discharge of the Yangtze River on PAHs sedimentation in the estuary. *Environmental Monitoring and Assessment, 189*, 10. https://doi.org/10.1007/s10661-016-5729-x.

Liu, H., Zhang, M., Lin, Z., & Xu, X. (2018). Spatial heterogeneity of the relationship between vegetation dynamics and climate change and their driving forces at multiple time scales in Southwest China. *Agricultural and Forest Meteorology, 256-257*, 10–21. https://doi.org/10.1016/j.agrformet.2018.02.015.

Ma, T. (2018). Quantitative responses of satellite-derived night-time lighting signals to anthropogenic land-use and land-cover changes across China. *Remote Sensing, 10*, 1447. https://doi.org/10.3390/rs10091447.

Ma, T. (2019). Spatiotemporal characteristics of urbanization in China from the perspective of remotely sensed big data of nighttime light. *Journal of Geo-Information Science (in Chinese), 21*(1), 59–67. https://doi.org/10.12082/dqxxkx.2019.180361.

Mora, C., Dousset, B., Caldwell, I. R., Powell, F. E., Geronimo, R. C., Bielecki, C. R., Counsell, C. W. W., Dietrich, B. S., Johnston, E. T., Louis, L. V., Lucas, M. P., McKenzie, M. M., Shea, A. G., Tseng, H., Giambelluca, T. W., Leon, L. R., Hawkins, E., & Trauernicht, C. (2017). Global risk of deadly heat. *Nature Climate Change, 7*, 501–506. https://doi.org/10.1038/nclimate3322.

Mu, S. J., Yang, H., Li, J. L., Chen Y.Z., Gang C.C., Zhou W., & Ju W.M. (2013). Spatio-temporal dynamics of vegetation coverage and its relationship with climate factors in Inner Mongolia, China. *Journal of Geographical Sciences, 23*(2), 231–246. https://doi.org/10.1007/s11442-013-1006-x .

Prajjwal, K. P., & Bardan, G. (2012). Time-series analysis of NDVI from AVHRR data over the Hindu Kush–Himalayan region for the period 1982–2006. *International Journal of Remote Sensing, 33*(21), 6710–6721. https://doi.org/10.1080/01431161.2012.692836.

Prince, S. D. (2010). Evidence from rain-use efficiencies does not indicate extensive Sahelian desertification. *Global Change Biology, 4*(4), 359–374. https://doi.org/10.1046/j.1365-2486.1998.00158.x.

Qu, S., Wang, L., Lin, A., Zhu, H., & Yuan, M. (2018). What drives the vegetation restoration in Yangtze River basin, China: climate change or anthropogenic factors? *Ecological Indicators, 90*, 438–450. https://doi.org/10.1016/j.ecolind.2018.03.029.

Shu, S., Yu, B. L., Wu, J. P., & Liu H., X. (2011). Methods for deriving urban built-up area using night-light data: assessment and application. *Remote Sensing Technology and Application (in Chinese), 26*(2), 169–176.

Verbesselt J, Hyndman R, Zeileis A, Culvenor D. (2010a). Phenological change detection while accounting for abrupt and gradual trends in satellite image time series. *Remote Sensing of Environment, 114*(12), 2970–2980. https://doi.org/10.1016/j.rse.2010.08.003

Verbesselt J., Hyndman R., Newnham G., & Culvenor D. (2010b). Detecting trend and seasonal changes in satellite image time series. *Remote Sensing of Environment, 114*(1), 106–115. https://doi.org/10.1016/j.rse.2009.08.014.

Wang, H., Liu, G. H., Li, Z. S., Ye X., Fu B.J., & Lv Y.H. (2018). Impacts of drought and human activity on vegetation growth in the grain for green program region, China. *Chinese Geographical Science, 28*, 470–481. https://doi.org/10.1007/s11769-018-0952-8 .

Wen, Z. F., Wu, S. J., Chen, J. L., & Lv M. Q. (2017). NDVI indicated long-term interannual changes in vegetation activities and their responses to climatic and anthropogenic factors in the Three Gorges Reservoir Region, China. *Science of The Total Environment., 574*, 947–959. https://doi.org/10.1016/j.scitotenv.2016.09.049 .

Wessels, K. J., Prince, S. D., Malherbe, J., Small, J., Frost, P. E., & VanZyl, D. (2007). Can human-induced land degradation be distinguished from the effects of rainfall variability? A case study in South Africa. *Journal of Arid Environments, 68*, 271–297. https://doi.org/10.1016/j.jaridenv.2006.05.015.

Wessels, K. J., Bergh, F. V. D., & Scholes, R. J. (2012). Limits to detectability of land degradation by trend analysis of vegetation index data. *Remote Sensing of Environment, 125*, 10–22. https://doi.org/10.1016/j.rse.2012.06.022.

Wu, J. S., Feng, Y. F., Zhang, X. Z., Susanne W., Britta T., Paolo T., & Song C.Q. (2017). Grazing exclusion by fencing non-linearly restored the degraded alpine grasslands on the Tibetan Plateau. *Scientific Reports, 7*, 15202. https://doi.org/10.1038/s41598-017-15530-2 .

Xu, L., Li, B., Yuan, Y., Gao, X., Zhang, T., & Sun, Q. (2016). Detecting different types of directional land cover changes using MODIS NDVI time series dataset. *Remote Sensing, 8*(6), 495. https://doi.org/10.3390/rs8060495.

Xu, L., Tu, Z., Zhou, Y., & Yu, G. (2018). Profiling human-induced vegetation change in the Horqin Sandy land of China using time series datasets. *Sustainability, 10*, 1068. https://doi.org/10.3390/su10041068.

Yuan, M., Wang, L., Lin, A., Liu, Z., & Qu, S. (2019a). Variations in land surface phenology and their response to climate change in Yangtze River basin during 1982–2015. *Theoretical and Applied Climatology., 137*, 1659–1674. https://doi.org/10.1007/s00704-018-2699-7.

Yuan, J., Xu, Y., Xiang, J., Wu, L., & Wang, D. (2019b). Spatiotemporal variation of vegetation coverage and its associated influence factor analysis in the Yangtze River Delta, eastern China. *Environmental Science and Pollution Research., 26*, 32866–32879. https://doi.org/10.1007/s11356-019-06378-2.

Zeileis, A. (2005). A unified approach to structural change tests based on ML scores, F statistics, and OLS residuals. *Econometric Reviews, 24*, 445–466. https://doi.org/10.1080/07474930500406053.

Zeileis, A., Leisch, F., Hornik, K., & Kleiber C. (2002). Strucchange: an R package for testing for structural change in linear regression models. *Journal of statistical Software, 7*, 27509. https://doi.org/10.18637/jss.v007.i02 .

Zeileis, A., Leisch, F., Kleiber, C., & Hornik, K. (2005). Monitoring structural change in dynamic econometric models. *Journal of Applied Econometrics, 20*, 99–121. https://doi.org/10.1002/jae.776.

Zhao, Y., He, C., & Zhang, Q. (2012). Monitoring vegetation dynamics by coupling linear trend analysis with change vector analysis: a case study in the Xilingol steppe in northern China. *International Journal of Remote Sensing, 33*, 287–308. https://doi.org/10.1080/01431161.2011.594102.

Zhao, X., Hu, H., Shen, H., Zhou, D., Zhou, L., Myneni, R. B., & Fang, J. (2015). Satellite-indicated long-term vegetation changes and their drivers on the Mongolian Plateau. *Landscape Ecology, 30*, 1599–1611. https://doi.org/10.1007/s10980-014-0095-y.

Zhu, Z., & Woodcock, C. E. (2013). Continuous change detection and classification of land cover using all available Landsat data. *Remote Sensing of Environment, 144*, 152–171. https://doi.org/10.1016/j.rse.2014.01.011.